Exciton oscillator strength in magnetic-field-induced spin superlattices CdTe/(Cd,Mn)Te

E. L. Ivchenko, A. V. Kavokin, V. P. Kochereshko, G. R. Posina, and I. N. Uraltsev
A. F. Ioffe Physico-Technical Institute, Russian Academy of Sciences, 194021 St. Petersburg, Russia

D. R. Yakovlev,* R. N. Bicknell-Tassius, A. Waag, and G. Landwehr
Physikalisches Institut der Universität Würzburg, 8700 Würzburg, Federal Republic of Germany
(Received 27 April 1992)

Resonance-reflectivity data on CdTe/(Cd,Mn)Te quantum wells and superlattices are analyzed to obtain the exciton longitudinal-transverse splitting or oscillator strength as a function of the layer widths and/or the band offsets altered by externally applied magnetic fields. A nonlocal-dielectric-response theory for single quantum wells and the concept of an optically homogeneous dielectric medium formulated for periodic structures are developed. Strong effects of the magnetic-field-induced type-I–type-II transition and the spin-superlattice formation for holes on the exciton oscillator strength are found to be in agreement with our calculations.

I. INTRODUCTION

Quasi-two-dimensional II-VI-semiconductor-based quantum-well (QW) structures, with their wide, direct band gaps, have potential applications as optoelectronic materials in the visible-light region. Their optical properties have been studied and rather small valence-band offsets and strong exciton effects have been demonstrated.[1–3] As a result of these characteristics, an additional confinement of holes is expected to arise due to the Coulomb interaction averaged over the electron distribution normal to the QW plane.[4–7]

The incorporation of diluted-magnetic-semiconductor barrier layers in QW structures, such as the model CdTe/(Cd,Mn)Te system, provides an exchange interaction between the spins of carriers that are essentially confined within the CdTe layers and those of the paramagnetic Mn^{2+} ions located within the (Cd,Mn)Te barrier layers. This has been demonstrated to cause a formation of the two-dimensional exciton magnetic polaron,[8,9] together with other spin-dependent effects of a large Faraday rotation[10] and the giant Zeeman splitting of the QW excitons associated with that of the band edges.[1–3,5,11] The latter effect has been intensively studied in evaluation of the valence-band offsets since it offers a unique opportunity to tune continuously the electronic bands and confining potentials through the application of external magnetic fields. However, to make a correct determination of the valence-band offset from the Zeeman-splitting analysis one has to take into account changes in the exciton binding energy as well as the effect of the Coulomb potential well on the hole confinement energy.[7]

In QW structures with low Mn content, the large Zeeman shift of the valence-band edge for a particular spin component may overcome the valence-band offset at moderate magnetic fields. This can lead to the transition from a type-I band alignment, where the electron and hole are confined to the same layer and their wave functions overlap substantially along the growth axis, to a type-II band alignment for the heterostructure with the electron and hole spatially separated and localized in different layers. As a result, the transition will change drastically the exciton binding energy and oscillator strength. The former effect has been evaluated from the Zeeman-shift analysis of the σ^+ component in $CdTe/Cd_{0.93}Mn_{0.07}Te$ multiple-quantum-well (MQW) structures.[2,7] The magnetic-field-induced localization of electrons and holes with the spin-up state in the nonmagnetic layers and those of opposite spin in the semimagnetic layers leads to formation of a spin superlattice with the same period as the structural superlattice (SL). The spin SL formation has been demonstrated by optical-transition-strength analyses in $ZnSe/Zn_{0.95}Mn_{0.05}Se$ (Ref. 12) and $ZnSe/Zn_{0.99}Fe_{0.01}Se$ (Ref. 13) MQW's.

In this paper we report our results of a resonance-reflectivity study of the confined exciton parameters as a function of the QW width in single-quantum-well (SQW) structures and of layer thicknesses in superlattices or as a function of barrier heights altered by the presence of an external magnetic field. Based on a nonlocal-dielectric-response theory developed for SQW structures and the concept of an optically homogeneous dielectric medium formulated for periodic heterostructures, we can analyze the resonance-reflectivity line shapes to measure the exciton resonance frequencies ω_0, longitudinal-transverse (LT) splitting ω_{LT}, and damping Γ. Throughout the paper we will concentrate on the exciton oscillator strength (or LT splitting) rather than on the other exciton parameters, since it is extremely sensitive to the shape of the exciton envelope wave function and to some relative redistribution of the electron and hole densities in excitons which are governed by the tuning of their confinement.

The organization of this paper is as follows. A theory of the exciton reflectivity, as well as calculations of the exciton LT splitting in SQW and SL structures, is developed in Sec. II. Experimental details are described in Sec. III. Experimental results and a comparison with calculations are given in Sec. IV. Effects of the type-I–type-II transition and spin-superlattice formation for

holes revealed in the exciton oscillator strength behavior are discussed. Conclusions appear in Sec. V.

II. THEORY

We will consider the light reflection from a single quantum well, multiple quantum wells, and a short-period superlattice. First, the resonance reflectivity will be connected with the exciton envelope function $\Psi_{\rm exc}(\mathbf{r}_e,\mathbf{r}_h)$ through the exciton oscillator strength or the longitudinal-transverse splitting $\omega_{\rm LT}$. Then, the function $\Psi_{\rm exc}$ as well as parameters $\omega_{\rm LT}^{\rm SQW}$, $\omega_{\rm LT}^{\rm MQW}$, and $\omega_{\rm LT}^{\rm SL}$ will be calculated for different limiting cases.

A. Reflection from a SQW

The amplitude coefficient $r=E_r/E_0$ for the reflection from a SQW structure shown in Fig. 1(a) is expressed in terms of the coefficient r_{123} of the reflection from layer 2 (quantum well) as follows:

$$r=\frac{r_{01}+r_{123}e^{i\phi}}{1+r_{01}r_{123}e^{i\phi}} . \tag{1}$$

Here r_{01} is the reflection coefficient at the boundary "vacuum-cap layer,"

$$\begin{aligned}&\phi=k_{1z}(2d_1+a) , \quad k_{1z}=k_1\cos\varphi_1 ,\\ &k_1=k_0\sqrt{\epsilon_b} , \quad \cos\varphi_1=\left[1-\frac{\sin^2\varphi_0}{\epsilon_b}\right]^{1/2} , \quad k_0=\frac{\omega}{c} ,\end{aligned} \tag{2}$$

φ_0 is the incidence angle, a is the QW width, ω is the light frequency, ϵ_b is the dielectric constant of the cap layer which is supposed to coincide with that of the layer 3 and with the background dielectric constant of the QW. In the vicinity of the exciton resonance frequency ω_0, the coefficient r_{123} for s- and p-polarized light is given by[14,15,17,18] (see also Ref. 16)

$$r_{123}^s=\frac{i\tilde{\Gamma}_s}{\tilde{\omega}_0-\omega-i(\Gamma+\tilde{\Gamma}_s)} , \tag{3a}$$

$$r_{123}^p=\frac{i\tilde{\Gamma}_p}{\tilde{\omega}_0-\omega-i(\Gamma+\tilde{\Gamma}_p)}-\frac{i\tilde{\Gamma}'_p}{\tilde{\omega}'_0-\omega-i(\Gamma+\tilde{\Gamma}'_p)} . \tag{3b}$$

Here the nonradiative exciton damping Γ is a parameter of the theory which is determined from a comparison with experiment, for the radiative exciton damping one obtains

$$\begin{aligned}&\tilde{\Gamma}_s=\frac{k_1^2a}{2k_{1z}}\omega_{{\rm LT},\perp}^{\rm SQW} , \quad \tilde{\Gamma}_p=\frac{k_{1z}^2}{k_1^2}\tilde{\Gamma}_s , \quad \tilde{\Gamma}'_p=\frac{k_x^2a}{2k_{1z}}\omega_{{\rm LT},\parallel}^{\rm SQW} ,\\ &k_x=k_0\sin\varphi_0 .\end{aligned} \tag{4}$$

For the simple conduction- and valence-band structure the oscillator strength (or the effective longitudinal-transverse splitting) for an exciton in a QW can be written as

$$\omega_{{\rm LT},\eta}^{\rm SQW}=\omega_{{\rm LT},\eta}\frac{\pi a_B^3}{a}\left[\int\phi(z)\cos(k_{1z}z)dz\right]^2 , \tag{5}$$

with

$$\begin{aligned}&\Phi(z)=\varphi_{\rm SQW}(0,z,z) ,\\ &\omega_{{\rm LT},\eta}a_B^3=\frac{4e^2P_{cv,\eta}^2}{\hbar\omega_0^2m_0^2\epsilon_b} ,\end{aligned} \tag{6}$$

where $\eta=\perp$ or $\parallel$, a_B is the exciton Bohr radius in a bulk crystal, the factor a_B^3 is introduced in Eqs. (5) and (6) for convenience, the interband matrix element of the momentum operator is defined by

$$P_{cv,\eta}^2=\sum_{s,m}|\langle cs|\hat{\mathbf{p}}\cdot\mathbf{e}_\eta|vm\rangle|^2 ,$$

$\mathbf{e}_\parallel\|z$, $\mathbf{e}_\perp\perp z$, s, and m are the spin indices of the electron states in the conduction (c) and valence (v) bands at the Γ point. The function $\varphi_{\rm SQW}(\boldsymbol{\rho},z_e,z_h)$ is connected with the exciton wave function according to

$$\Psi_{\rm SQW}(\mathbf{r}_e,\mathbf{r}_h)=\frac{1}{\sqrt{S}}\exp\{i(k_xX+k_yY)\}\varphi_{\rm SQW}(\boldsymbol{\rho},z_e,z_h) , \tag{7}$$

$\rho_x=x_e-x_h$, $\rho_y=y_e-y_h$, X and Y are the exciton center-of-mass coordinates, S is the heterostructure area in the (x,y) plane. The frequencies $\tilde{\omega}_0$ and $\tilde{\omega}'_0$ are the exciton resonance frequencies renormalized due to the exciton interaction with the electromagnetic field

$$\begin{aligned}\tilde{\omega}_0&=\omega_0+\tfrac{1}{2}k_z\omega_{{\rm LT},\perp}\pi a_B^3\\ &\quad\times\int dz\int dz'\Phi(z)\Phi(z')\sin(k_{1z})|z-z'| ,\\ \tilde{\omega}'_0&=\omega_0+\omega_{{\rm LT},\parallel}\pi a_B^3\int\Phi^2(z)dz+(k_x/k_{1z})^2(\tilde{\omega}_0-\omega_0) .\end{aligned}$$

The resonance frequency renormalization and the pres-

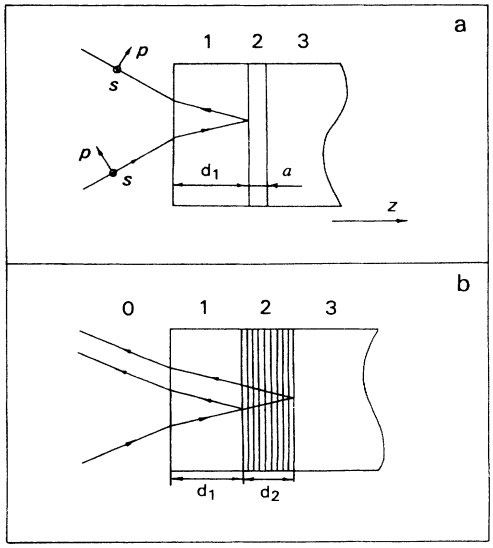

FIG. 1. Schematic illustration of reflection at oblique incidence of light with polarization in the incidence plane (p) or normal to that (s) from a single-quantum-well structure (a) and a superlattice or multiple-quantum-well structure (b).

ence of $\tilde{\Gamma}$ in the denominators of Eqs. (3a) and (3b) are two different polaritonic effects for excitons in a SQW. It is appropriate to mention here that the effect of retarding electron-photon interaction on exciton spectra in the one- and two-dimensional crystals has been analyzed in Ref. 19.

If mixing between the heavy- and light-hole states is neglected, then we have for the $e1$-hh1 ($1s$) excitons

$$P_{cv,\perp}^2=|\langle S|\hat{p}_z|Z\rangle|^2\ ,\quad P_{cv,\parallel}^2=0 \tag{8a}$$

and for the $e1$-lh1 ($1s$) excitons

$$P_{cv,\perp}^2=\tfrac{1}{4}P_{cv,\parallel}^2=\tfrac{1}{3}|\langle S|\hat{p}_z|Z\rangle|^2\ , \tag{8b}$$

where $S(\mathbf{r})$ and $X(\mathbf{r})$, $Y(\mathbf{r})$, $Z(\mathbf{r})$ are the Γ-point Bloch functions of the symmetry Γ_1 and Γ_{15}.

It is instructive to compare Eq. (3a) [or (3b)] with the reflection coefficient $r_{123}^{\rm eff}$ from a layer of thickness a characterized by a local dielectric function

$$\epsilon(\omega)=\epsilon_b+\frac{\epsilon_b\omega_{\rm LT}^{\rm eff}}{\omega_0-\omega-i\Gamma}$$

and incorporated in a medium with the dielectric constant ϵ_b. For $k_{1z}a\ll 1\ll\epsilon_b$ and $\omega_{\rm LT}^{\rm eff}\ll\Gamma$, r_{123} and $r_{123}^{\rm eff}$ coincide if we set

$$\omega_{{\rm LT},\eta}^{\rm eff}=\omega_{{\rm LT},\eta}\frac{\pi a_B^3}{a}\left[\int\Phi(z)dz\right]^2\ . \tag{9}$$

In this case $\tilde{\Gamma}_{s,p},\tilde{\Gamma}'_p\ll\Gamma$ and the denominators in Eqs. (3a) and (3b) can be reduced to $\omega_0-\omega-i\Gamma$.

B. Reflection from a periodic heterostructure

Let us consider now a regular MQW structure, i.e., a set of QW's separated by barriers thick enough to make them impenetrable for free carriers. While, from the viewpoint of the electronic properties, each of these wells is isolated, the presence of many wells affects noticeably the optical characteristics of the structure. In the approximation of an optically homogeneous dielectric medium the response of such a structure can be described by the dielectric tensor with components[17,20]

$$\begin{aligned}\epsilon_{xx}=\epsilon_{yy}\equiv\epsilon_\perp(\omega)&=\epsilon_b+\frac{\epsilon_b\omega_{{\rm LT},\perp}^{\rm MQW}}{\omega_0-\omega-i\Gamma}\ ,\\ \epsilon_{zz}\equiv\epsilon_\parallel(\omega)&=\epsilon_b+\frac{\epsilon_b\omega_{{\rm LT},\parallel}^{\rm MQW}}{\omega_0'-\omega-i\Gamma}\ ,\end{aligned} \tag{10}$$

where

$$\begin{aligned}\omega_{{\rm LT},\eta}^{\rm MQW}&=\frac{a}{a+b}\omega_{{\rm LT},\eta}^{\rm SQW}\ ,\\ \omega_0'&=\omega_0+\omega_{{\rm LT},\parallel}\pi a_B^3\int\Phi^2(z)dz-\omega_{{\rm LT},\parallel}^{\rm MQW}\ ,\end{aligned} \tag{11}$$

b is the barrier thickness and $\omega_{{\rm LT},\eta}^{\rm SQW}$ is introduced in Eq. (5). It has been shown[17] that the criteria for the validity of the homogeneous-medium approximation are as follows:

$$k_1(a+b)\ll 1 \tag{12a}$$

and

$$\left[\frac{a+b}{\lambda}\right]^2\epsilon_b\frac{\omega_{\rm LT}^{\rm MQW}}{\Gamma}\ll 1\ , \tag{12b}$$

where λ is the light wavelength in vacuum. Note that the criterion (12b) differs from the more stringent condition $\omega_{\rm LT}^{\rm MQW}\ll\Gamma$ discussed in Refs. 16 and 21. Thus, if the conditions (12a) and (12b) are satisfied, then $\omega_{\rm LT}^{\rm MQW}$ is the longitudinal-transverse splitting for excitons in MQW's in the same sense as a similar notion used for A or B excitons in CdS or CdSe bulk crystals (see, e.g., Ref. 22).

The amplitude reflection coefficient for the structure shown in Fig. 1(b) is defined by expression (1), where one has to set $\phi=2k_{1z}d_1$ and

$$r_{123}=\frac{1-\exp(2i\phi_2)}{1-r_{12}^2\exp(2i\phi_2)}r_{12}\ . \tag{13}$$

Here $\phi_2=k_{2z}d_2$ and r_{12} is the reflection coefficient at the boundary between layers 1 and 2. For p-polarized light,

$$k_{2z}=k_0\left[\epsilon_\perp\left[1-\frac{\sin^2\varphi_0}{\epsilon_\parallel}\right]\right]^{1/2}$$

and

$$r_{12}=-\frac{\cos\varphi_1\sqrt{\epsilon_\perp}-[\epsilon_b(\epsilon_\parallel-\sin^2\varphi_0)/\epsilon_\parallel]^{1/2}}{\cos\varphi_1\sqrt{\epsilon_\perp}+[\epsilon_b(\epsilon_\parallel-\sin^2\varphi_0)/\epsilon_\parallel]^{1/2}}\ . \tag{14}$$

According to Eqs. (6) and (7a) the $e1$-hh1 ($1s$) excitons are dipole-moment inactive in the polarization $e\|z$, i.e., $\omega_{{\rm LT},\parallel}^{\rm MQW}=0$ and $\epsilon_\parallel=\epsilon_b$ [see Eq. (9)]. In this case r_{12} reduces to

$$r_{12}=-\frac{\sqrt{\epsilon_\perp}-\sqrt{\epsilon_b}}{\sqrt{\epsilon_\perp}+\sqrt{\epsilon_b}} \tag{14a}$$

and becomes independent of the incidence angle φ_0.

Equations (1) and (12) are valid also for the description of reflection from a structure with a short-period SL. Since in this case the electron motion is three dimensional, the longitudinal-transverse splitting $\omega_{\rm LT}^{\rm SL}$ differs from the parameter $\omega_{\rm LT}^{\rm MQW}$ in Eq. (9) and cannot be expressed in terms of $\omega_{\rm LT}^{\rm SQW}$ by the simple relation (11).

C. Longitudinal-transverse splitting in a SQW

The exciton envelope wave function $\varphi_{\rm SQW}$ given by Eq. (7) can be represented as

$$\varphi_{\rm SQW}(\boldsymbol{\rho},z_e,z_h)=f\boldsymbol{\rho}U_e(z_e)U_h(z_h)\ , \tag{15}$$

where $f(\boldsymbol{\rho})$ describes the relative motion of the electron and hole in the QW plane.

At the bottom of the subband $e1$ or hh1, $U_n(z)$ is an even function given as follows:

$$U_n(z)=\begin{cases}C_n\cos(k_nz) & \text{for } |z|<a/2\\ D_n\exp[-\chi_n(|z|-a/2)] & \text{for } |z|>a/2\ .\end{cases} \tag{16}$$

Here $k_n=(2m_n^aE_n/\hbar^2)^{1/2}$, $\chi_n=[2m_n^b(V_n-E_n)/\hbar^2]^{1/2}$, E_n is the confinement energy of a conduction electron ($n=e$) or heavy hole ($n=$hh), $m_n^{a,b}$ is the electron or heavy-hole effective mass in the corresponding bulk semi-

conductor, a and b being the indices of well and barrier layers, V_e and V_{hh} are the offsets of the conduction and valence bands, respectively.

For the boundary conditions with continuity of $U_n(z)$ and $m_n^{-1}dU_n(z)/dz$, C_n and D_n can be written explicitly as

$$C_n=\left[\frac{a}{2}\left[1+\frac{\sin(k_n a)}{k_n a}+\frac{1+\cos(k_n a)}{\chi_n a}\right]\right]^{-1/2},$$
$$D_n=C_n\cos(k_n a/2)\ . \tag{17}$$

Following Ref. 20 and using Eqs. (9) and (16), we obtain for $k_1 a \ll 1$,

$$\frac{\omega_{LT}^{SQW}}{\omega_{LT}}=\frac{\pi a_B^3}{a}f^2(0)I_{eh}^2\ , \tag{18}$$

where $\omega_{LT}\equiv\omega_{LT,\perp}$ and $I_{eh}=\int dz\, U_e(z)U_h(z)$. The overlap integral can be conveniently represented as $I_{eh}^a+I_{eh}^b$, where

$$I_{eh}^a=C_e C_h\left\{\frac{\sin[(k_e+k_{hh})a/2]}{k_e+k_{hh}}+\frac{\sin[(k_e-k_{hh})a/2]}{k_e-k_{hh}}\right\},$$
$$I_{eh}^b=\frac{2D_e D_h}{\chi_e+\chi_{hh}}\ . \tag{19}$$

In the adiabatic approximation for the $1s$ exciton the relative motion wave function $f(\rho)$ satisfies the two-dimensional Schrödinger equation

$$\left\{-\frac{\hbar^2}{2\mu_\perp}\frac{1}{\rho}\frac{d}{d\rho}\left[\rho\frac{d}{d\rho}\right]+v(\rho)\right\}f(\rho)=E_{exc}f(\rho) \tag{20}$$

with the effective potential

$$v(\rho)=-\frac{e^2}{\epsilon_b}\int dz_e\int dz_h\frac{U_e^2(z_e)U_h^2(z_h)}{\sqrt{\rho^2+(z_e-z_h)^2}}\ . \tag{21}$$

Here $\mu_\perp=m_e^\perp m_{hh}^\perp/(m_e^\perp+m_{hh}^\perp)$ is the reduced effective mass, $m_n^\perp$ is the transverse (in-plane) effective mass of an electron or a hole, $-E_{exc}$ is the exciton binding energy. To solve Eq. (20) we apply the variational approach with a trial function of the form

$$f(\rho)=\left[\frac{2}{\pi}\right]^{1/2}\frac{1}{a_B}\exp\left[-\frac{\rho}{a_B}\right], \tag{22}$$

where a_B is a variational parameter.

Minimizing the energy $E_{exc}(a_B)$ we obtain the equation for the optimal value of a_B:

$$\int_0^\infty d\rho\,\rho v(\rho)\left[1-\frac{\rho}{a_B}\right]\exp\left[-\frac{2\rho}{a_B}\right]=-\frac{\hbar^2}{8\mu_\perp}\ . \tag{23}$$

For the two-dimensional (2D) Coulomb potential $v_{2D}(\rho)=-e^2/(\epsilon_b\rho)$, Eq. (23) provides $a_B\equiv a_B^{(2D)}=\hbar^2\epsilon_b/2\mu_\perp e^2$.

In the following, we also use the modification of the above procedure taking account of an additional heavy-hole confinement along the z direction due to the adiabatic Coulomb potential created by the electron in the exciton.[4,7] In this case $f(\rho)$ and the hole envelope function $U_h(z)$ in Eq. (19) for φ_{SQW} can be found as a self-consistent solution of the set of Eq. (20) and equation

$$\left[-\frac{\hbar^2}{2m_{hh}^\parallel}\frac{d^2}{dz^2}+V_h(z)+w(z)\right]U_h(z)=E_h U_h(z)\ , \tag{24}$$

where

$$w(z_h)=-\frac{e^2}{\epsilon_b}\int\int\frac{U_e^2(z_e)f^2(\rho)}{\sqrt{\rho^2+(z_e-z_h)^2}}2\pi\rho\,d\rho\,dz_e\ , \tag{25}$$

$V_h(z)=V_{hh}\Theta(|z|-a/2)$ and $\Theta(x)$ is the steplike Heaviside function. Following Ref. 4 we approximate the hole confinement potential by a parabola (harmonic-oscillator potential). In this case $U_h(z)$ has a Gaussian form

$$U_h(z)=\left[\left[\frac{\pi}{2}\right]^{1/2}L_h\right]^{-1/2}\exp\left\{-\left[\frac{z}{L_h}\right]^2\right\},$$
$$L_h=\left[\frac{\hbar a_B}{8e}\left[\frac{\epsilon_b a}{m_{hh}^\parallel}\right]^{1/2}\right]^{1/2}, \tag{26}$$

where $m_{hh}^\parallel$ is the heavy-hole effective mass in the z direction. Estimations show that for $CdTe/Cd_{1-x}Mn_xTe$ QW's the parabolic approximation of the hole confinement potential is valid for $a>28$ and 33 Å if $x=0.25$ or 0.1, respectively.

D. Longitudinal-transverse splitting in a SL

For a short-period SL with wide minibands the electron motion becomes three dimensional, the longitudinal-transverse splitting can be calculated by

$$\frac{\omega_{LT}^{SL}}{\omega_{LT}}=\pi a_B^3 J_{eh}^2 f_{SL}^2(0)\ . \tag{27}$$

Here $f_{SL}(\mathbf{r})$ is the relative motion wave function of an exciton in the SL, $\mathbf{r}=\mathbf{r}_e-\mathbf{r}_h$, J_{eh} is the overlap integral of the periodic (super-Bloch) amplitudes at the bottom of the electron- and heavy-hole minibands. In the generalized Kronig-Penney model we have

$$J_{eh}=J_{eh}^a+J_{eh}^b\ ,$$
$$J_{eh}^a=\tilde{C}_e\tilde{C}_h\left\{\frac{\sin[(k_e+k_{hh})a/2]}{k_e+k_{hh}}+\frac{\sin[(k_e-k_{hh})a/2]}{k_e-k_{hh}}\right\},$$
$$J_{eh}^b=\tilde{D}_e\tilde{D}_h\left\{\frac{\sinh[(\chi_e+\chi_{hh})b/2]}{\chi_e+\chi_{hh}}+\frac{\sinh[(\chi_e-\chi_{hh})b/2]}{\chi_e-\chi_{hh}}\right\}. \tag{28}$$

$\tilde{C}_n$ and $\tilde{D}_n$ are defined by

$$\tilde{C}_n=\sqrt{2}\left[a+\frac{\sin(k_n a)}{k_n}+\frac{1+\cos(k_n a)}{1+\cosh(\chi_n b)}\left[b+\frac{\sinh(\chi_n b)}{\chi_n}\right]\right]^{-1/2},$$

$$\tilde{D}_n=\tilde{C}_n\frac{\cos[k_n a/2]}{\cosh[\chi_n b/2]}.$$

The relative electron-hole motion can be approximated fairly well by a trial wave function

$$f_{\mathrm{SL}}(\mathbf{r})=(\pi a_{\parallel}a_{\perp}^2)^{-1/2}\times\exp\{-[(\rho/a_{\perp})^2+(z_e-z_h)^2/a_{\parallel}^2]^{1/2}\}, \quad (29)$$

with the variational parameters $a_{\parallel}$ and $a_{\perp}$.[23]

It should be mentioned that the interband matrix elements P_{cv}^a, P_{cv}^b in well and barrier layers are different in the general case. This difference can be taken into account if we replace P_{cv} by P_{cv}^a in Eq. (6) and $I_{\mathrm{eh}},J_{\mathrm{eh}}$ by

$$I_{\mathrm{eh}}^a+\frac{P_{cv}^b}{P_{cv}^a}I_{\mathrm{eh}}^b,\quad J_{\mathrm{eh}}^a+\frac{P_{cv}^b}{P_{cv}^a}J_{\mathrm{eh}}^b$$

in Eqs. (18) and (27).

E. Semimagnetic heterostructure in the presence of external magnetic fields

In heterostructures with semimagnetic barriers, a longitudinal magnetic field $\mathbf{H}\|z$ changes the band offsets by

$$\Delta V_e^s(H_z)=-\frac{\alpha}{v_0}\tilde{x}s\langle S_z\rangle,$$
$$\Delta V_{\mathrm{hh}}^m(H_z)=-\frac{\beta}{3v_0}\tilde{x}m\langle S_z\rangle. \quad (30)$$

Here $v_0=a_0^3/4$ is the unit cell volume (in CdTe the lattice constant $a_0=6.48$ Å), α and β are the constants of exchange interaction between the conduction/valence states and magnetic ions, $S=\pm\frac{1}{2}$ and $m=\pm\frac{3}{2}$ are the electron and heavy-hole spins, $\langle S_z\rangle$ is the thermal average of a magnetic ion spin.

For $CdTe/Cd_{1-x}Mn_xTe$ system we have

$$\langle S_z\rangle=\tfrac{5}{2}B_{5/2}(5g\mu_B H_z/2k_B(T+T_{\mathrm{AF}})), \quad (31)$$

μ_B being the Bohr magneton, g the $Mn^{2+}(3d^5)$ ion g factor, and $B_{5/2}$ the Brillouin function. According to Ref. 24 $\alpha/v_0=220$ meV, $\beta/v_0=880$ meV, and $g\simeq 2$.

In order to take into account the antiferromagnetic Mn-Mn spin coupling we have introduced in Eqs. (30) and (31) two fitting parameters: the effective manganese content $\tilde{x}$ an the antiferromagnetic shift of temperature, T_{AF}.[24] In the paramagnetic phase $\tilde{x}=x$ and $T_{\mathrm{AF}}=0$, whereas in the spin-glass phase $\tilde{x}<x$ and $T_{\mathrm{AF}}>0$. This reflects the antiferromagnetic interaction resisting the Mn^{2+} spin alignment along the magnetic-field direction.

The dependence of band offsets $V_e+\Delta V_e^s$, $V_{\mathrm{hh}}+\Delta V_{\mathrm{hh}}^m$ on s and m results in the spin splitting of the electron and hole QW subbands or SL minibands. Therefore, the exciton states $|s,m\rangle$ are also split.

At normal incidence the light is reflected in the diagonal circular configuration (σ_+,σ_+) or (σ_-,σ_-). In this case, the reflection coefficient r_{123} is given by

$$r_{124}^{\sigma_\pm}=\frac{i\tilde{\Gamma}_\pm}{\tilde{\omega}_0^{\pm}-\omega-i(\Gamma_\pm+\tilde{\Gamma}_\pm)}, \quad (32)$$

where $\tilde{\omega}_0^{\pm}$, $\Gamma_\pm$, and $\tilde{\Gamma}_\pm$ are the resonance frequencies, nonradiative and radiative dampings of the QW exciton states with $j=s+m=\pm 1$.

In the presence of a longitudinal magnetic field the effective dielectric tensor $\epsilon_{\alpha\beta}$ of a MQW structure or a SL is diagonal in the basis (σ_+,σ_-,z) with

$$\epsilon_{\sigma_\pm\sigma_\pm}(\omega)=\epsilon_b+\frac{\epsilon_b\omega_{\mathrm{LT}}(\sigma_\pm)}{\omega_0^{\pm}-\omega-i\Gamma_\pm}, \quad (33)$$

where $\omega_{\mathrm{LT}}(\sigma_\pm)$ can be identified as an oscillator strength for excitons with the angular momentum $j=+1$ or -1 and are calculated in accordance with Eqs. (11) or (18).

III. EXPERIMENTAL DETAILS

$CdTe/Cd_{1-x}Mn_xTe$ SQW structures and superlattices were grown by molecular beam epitaxy on (100) CdTe substrates followed by CdTe buffer layers and 6000-Å $Cd_{1-x}Mn_xTe$ layers.[25] The structures contained either a set of SQW's separated by 1000-Å-thick barrier layers or 50-period SL's with equal widths of well and barrier layers. The SQW width a and the SL period $a+b=2a$ ranged from 6 to 300 Å and from 24 to 120 Å, respectively. The manganese content in the barrier layers was $x\approx 0.25$ or 0.1. The lattice mismatch between the $Cd_{1-x}Mn_xTe$ barriers and the CdTe wells is approximately 0.5% and 0.2% for the above contents, respectively. Our structures are expected to be relaxed and thin CdTe SQW's strained to the $Cd_{1-x}Mn_xTe$ barriers while in the SL's both the well and barrier layers are strained. A comparison of the heavy- and light-hole exciton splittings in single and multiple quantum wells of equal widths has demonstrated that the strain-induced splittings appear to be smaller than energies of the electron and hole quantization.

Reflection spectroscopy has been performed at pumped-liquid-He temperature of 1.6 K. Reflection spectra were taken at the Brewster-angle geometry with light polarization in the incidence plane or at the normal-incident geometry. Photoluminescence spectra were excited using an argon-ion laser (514.4 nm). A 2.5-m double monochromator with cooled photomultiplier and associated photon counting system were used for data acquisition. The magnetic field was applied in the Faraday geometry parallel to the structure axis [100] by using a superconducting magnet up to 7 T. In this case reflection was taken at normal-incidence geometry and analyzed in circular polarizations.

IV. RESULTS AND DISCUSSIONS

A. Exciton resonance reflectivity

Resonances attributed to the heavy- and light-hole exciton ground states from SQW's of different widths dom-

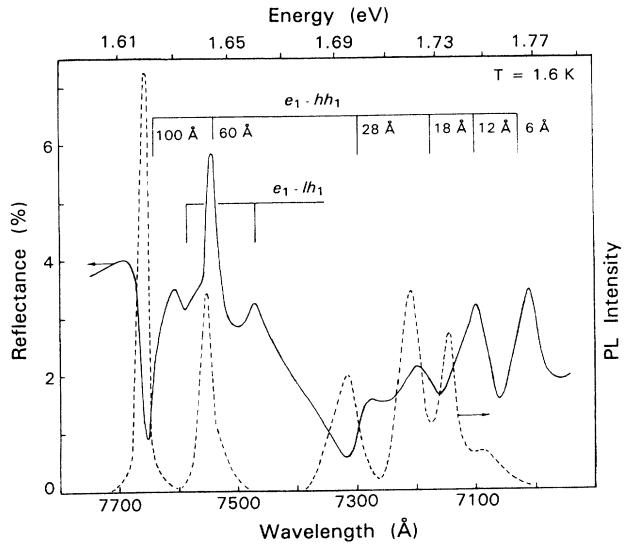

FIG. 2. Photoluminescence (dashed) and reflection (solid) spectra taken from the $CdTe/Cd_{0.9}Mn_{0.1}Te$ SQW structure at an incidence angle of 74° in p polarization. SQW widths ranged from 100 to 6 Å. Arrows indicate the resonance energies of the heavy- and light-hole excitons evaluated from the reflectivity line-shape analysis.

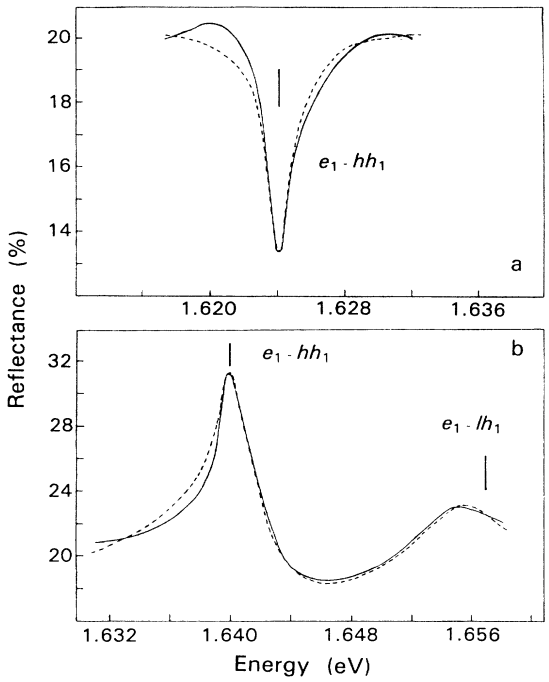

FIG. 3. Normal incidence reflection spectra (solid) in the heavy- and light-hole ground-state excitons region taken from $CdTe/Cd_{0.9}Mn_{0.1}$ Te structures with an 80-Å-thick SQW (a) and a 120-Å period MQW (b). Calculated spectra (dashed) are fitted with $\hbar\omega_0^{hh}=1.624$ eV, $\hbar\omega_{LT}^{hh}=1.25$ meV, $\hbar\Gamma^{hh}=1.10$ meV, $\epsilon_b=9.9$ for SQW and with $\hbar\omega_0^{hh}=1.640$ eV, $\hbar\omega_0^{lh}=1.657$ eV, $\hbar\omega_{LT}^{hh}=1.10$ meV, $\hbar\omega_{LT}^{lh}=1.0$ meV, $\hbar\Gamma^{hh}=1.50$ meV, $\hbar\Gamma^{lh}=4.1$ meV, $\epsilon_b=9.6$ for MQW.

inate the overall reflection spectrum taken in p polarization at incidence angles close to the Brewster angle, as shown by the solid line in Fig. 2. Neither an influence of the light-hole resonance in thin SQW's nor effects of other excited states on the heavy-hole exciton resonance line shape are expected since these resonances are hardly resolved from the background reflectivity of the SQW structures. Intense luminescence peaks of the heavy-hole excitons photoexcited above the band gap of the $Cd_{1-x}Mn_xTe$ barriers, shown by the dashed line in Fig. 2, appear to be redshifted from those resonance frequences measured by the reflectivity line-shape analysis and indicated by arrows. The redshifts result from an exciton localization on the one-monolayer fluctuations of the QW width. Since the QW width fluctuations change the electron and hole confinement energies,[25] their contribution to broadening of the exciton resonance reflectivity line shapes dominates in thin QW's and is described in Sec. II by the exciton nonradiative damping Γ. A substantial increase in the broadening with a decrease in the QW width is observed in agreement with the theoretical dependence of confinement energies on the QW width.

Figure 3(a) displays the heavy-hole exciton reflection spectrum taken from a 80-Å-thick SQW at the normal-incidence geometry (solid line) together with that calculated (dashed) in the approximation developed in Sec. II A. Three parameters were used in the fitting procedure: (i) the resonance frequency ω_0, evaluated from the resonance spectral position and the line-shape phase analysis; (ii) the exciton damping Γ; and (iii) the longitudinal-transverse splitting, ω_{LT}^{SQW}, which governs both the line-shape half-width and amplitude. The confinement effect provides $\hbar\omega_{LT}^{SQW}=1.25$ meV, which exceeds by approximately a factor of 2 the value for excitons in bulk CdTe. Note that in this SQW $\hbar\Gamma=1.1$ meV is even less than the $\hbar\omega_{LT}$ value. As far as we know, this is the first observed spectrum in quantum-well structures with the ratio $\omega_{LT}/\Gamma>1$. According to Eq. (4) for a SQW structure the strength of exciton-polaritonic effects is determined by the parameter

$$\frac{\tilde{\Gamma}}{\Gamma}=\frac{k_1 a}{2}\frac{\omega_{LT}^{SQW}}{\Gamma},$$

which remains for $a=80$ Å rather small to make polaritonic effects noticeable. However, in a MQW structure with $\omega_{LT}/\Gamma\sim 1$ and $a\sim b$, one could observe pronounced effects specific for exciton polaritons in the bulk crystals (see Ref. 19).

The heavy- and light-hole exciton reflection spectrum taken from a 60/60-Å MQW structure is shown by the solid line in Fig. 3(b). The best fit to the calculated curve (dashed line) is obtained with $\omega_{LT}/\Gamma\sim 0.7$ for the heavy-hole exciton. This ratio is very close to the criterium of the polariton effect manifestation. Therefore, we conclude that the II-VI MQW structures are real candidates for the demonstration of the superlattice polaritonic effect. It is worth noting that this criterium is hardly satisfied for the III-V MQW structures where the ω_{LT}^{MQW} value is less by a factor of 3 when compared to those in $CdTe/Cd_{0.9}Mn_{0.1}Te$ MQW's.[20]

The excellent agreement obtained between the experi-

mental and theoretical resonance reflectivity allows us to determine accurately the heavy-hole exciton parameters as a function of the QW width. Figure 4 displays the dependences of the effective longitudinal-transverse splitting on the SQW width for two contents $x=0.1$ (a) and 0.25 (b) of the $Cd_{1-x}Mn_xTe$ barriers. $\hbar\omega_{LT}^{SQW}$ is normalized to $\hbar\omega_{LT}^{bulk}=0.67$ meV measured in 300-Å-thick SQW's, which coincides with the LT splitting derived from the polariton interference experiments on bulk CdTe layers.[26] The LT splitting shows a slow monotonic increase in the range of QW widths down to 30 Å and a dramatic enhancement for thinner wells which tends to saturate or even to turn back in the thinnest QW's ($a<18$ Å) for $x=0.1$ or 0.25, respectively.

The figure also includes results of our calculations using three different models: (i) for the 2D Coulomb electron-hole potential determined by $-e^2/(\epsilon_b\rho)$, as shown by solid lines; (ii) for the quasi-2D Coulomb potential given by Eq. (21), as shown by dashed lines; and (iii) in the parabolic approximation for the adiabatic hole confinement potential (dotted lines). In the calculations, we assume $V_{hh}^0\approx 0.12\Delta E_g$ and take into account the strain-induced valence-band offsets of 4.5 or 11 meV for $x=0.1$ or 0.25, respectively.[27] This provides barrier heights for heavy holes of 23 and 59 meV for the above contents. Neglecting the differences between the effective masses in the well and barrier layers, we take $m_e^{a,b}=0.09m_0$ and $m_{hh}^{a,b}=0.5m_0$ in the structures with $x=0.1$. In the case of $x=0.25$, the barrier effective masses are taken $m_e^b=0.15m_0$ and $m_{hh}^b=0.75m_0$.

For QW's thicker than 32 Å the data appear to be in excellent agreement with the predictions of the third model and to indicate that the hole is subject to the combined effective potential with a dominant contribution from the adiabatic Coulomb potential. The dramatic enhancement of the LT splitting by more than a factor of 30 (15) observed in the thinner wells of $x=0.25$ ($x=0.10$) structures seems to be in line with the predictions of the first model and governed by the ω_{LT}^{SQW} (a^{-1}) dependence [see Eq. (9)]. In the narrowest QW's, the deviation of the effective potential $v(\rho)$ from the 2D Coulomb potential provides a limitation of this increase. Taking into account the transition from the 2D to 3D character of the exciton wave function due to its substantial penetration into the barrier layers, the second model explains qualitatively the observed behavior of the LT splitting as a result of the corresponding increase in the in-plane exciton Bohr radius.

In Fig. 5 the normalized longitudinal-transverse splitting of the heavy-hole exciton is shown as a function of the SL period for the $x=0.1$ (open circles) and 0.25 (closed circles) periodic structures. The observed nonmonotonic behavior is characteristic of the 2D-3D transition for the exciton wave function. The transition occurs when a period decreases down to 60 Å. The exciton confinement effect governs an increase in the LT splitting for MQW's with barrier widths down to 35 Å. A decrease of the $\hbar\omega_{LT}$ values in SL's with shorter periods indicates that the exciton wave function spreads at least through several SL layers. Figure 5 also includes results of our calculations assuming the above set of parameters and using Eqs. (11), (18), or (27) for MQW or SL structures with $x=0.1$ (0.25) as shown by dotted (dashed-dotted) or dashed (solid) lines, respectively. The values of ω_{LT}^{SQW} connected with the ω_{LT}^{MQW} by Eq. (10) were calculated taking into account a shrinkage of the hole envelop function $U_h(z)$ described by Eq. (26).

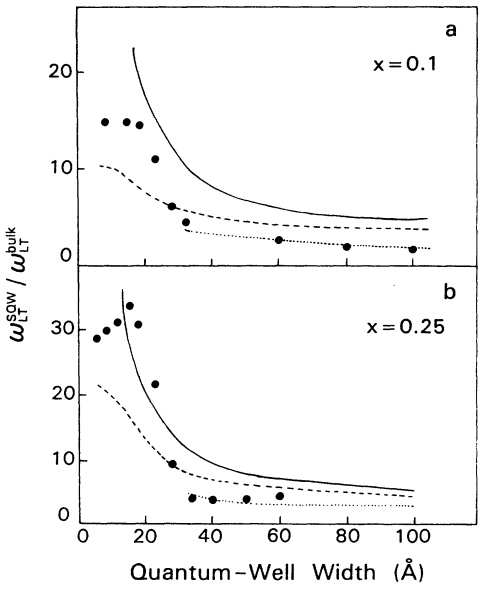

FIG. 4. The longitudinal-transverse splitting of the heavy-hole exciton normalized to that of the exciton in bulk CdTe (closed circles) as a function of well width a in SQW structures with $x=0.1$ (a) and 0.25 (b). Calculations with the 2D-Coulomb electron-hole potential (solid line), quasi-2D-Coulomb potential (dashed), and in the parabolic approximation for the adiabatic hole confinement potential (dotted) with parameters explained in text.

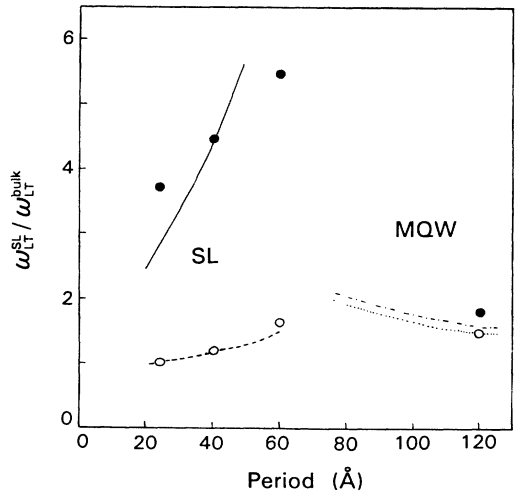

FIG. 5. The normalized longitudinal-transverse splitting of the heavy-hole exciton as a function of a period in regular structures with equal width of the well and barrier layers and $x=0.1$ (open circles) and 0.25 (closed circles). Theoretical curves are computed for MQW's with the use of Eqs. (11) and (18) for $x=0.1$ (dotted line), 0.25 (dashed-dotted), and for SL's with the use Eq. (27) for $x=0.1$ (dashed) and 0.25 (solid).

In agreement with the theoretical prediction [see Eq. (10)] the measured values of ω_{LT}^{MQW} (Fig. 5) and ω_{LT}^{SQW} (Fig. 4) differ by a factor of $\frac{1}{2}$, which is nothing else than the ratio $a/(a+b)$ at $a=b$. The values of LT splittings in the $x=0.1$ SL's are weakly dependent on the SL period and are close to the bulk value signaling the 3D character of the exciton wave function due to an existence of both the electron- and heavy-hole minibands. While a strong reduction of ω_{LT}^{SL} observed with period decrease in the $x=0.25$ SL's is governed by the electron miniband formation.

B. Magnetic tuning of exciton parameters

By altering the barrier heights substantially by external magnetic fields, one has the opportunity to study changes of the dimensionality of the exciton wave function and the type of the 2D heterostructures, monitoring the exciton parameters for particular spin components as a function of the magnetic field. The hole contribution to the exciton Zeeman splitting dominates because of the smaller value of the electron exchange constant in comparison to that of holes.[24] The effects are expected to occur in structures with $Cd_{0.9}Mn_{0.1}Te$ barriers where the Zeeman splitting of the valence-band states at moderate fields exceeds the valence-band offset at zero field.

The Zeeman splittings of the heavy-hole exciton states $|-\frac{1}{2},\frac{3}{2}\rangle$ and $|\frac{1}{2},-\frac{3}{2}\rangle$ measured at magnetic fields parallel to the growth axis are shown in Fig. 6 for a 18-Å-thick SQW (a) and for a 40-Å-period SL (b). The figure also includes results of our calculations with the use of Eq. (30) and the above set of band parameters for $x=0.1$ with $T_{AF}=2.4$ K and $\bar{x}=0.05$ or 0.07 for the SQW and SL, respectively, shown by solid lines.

According to Eqs. (30) and (31), the offset of the heavy-hole state $m=\frac{3}{2}$ vanishes at the magnetic field H_0 that satisfied the equation

$$\frac{\beta}{2v_0}\bar{x}\langle S_z\rangle = V_{hh} \ . \tag{34}$$

For the assumed value of $V_{hh}=23$ meV, we find $H_0=1.3$ T. Any further increase of the magnetic field causes heavy-hole localization in the barrier layers. Observing in the SQW a reduction of the σ^+-component shift in comparison to that calculated [dashed line in Fig. 6(a)], one could assign this behavior to a decrease of the exciton binding energy due to the type-I–type-II transition for heavy holes. However, the hole confinement to an additional adiabatic Coulomb potential is expected to shift a manifestation of the transition to higher fields. To take into account both of these effects on the exciton Zeeman splitting in SQW's it is necessary to carry out variational calculations.[7]

The 3D character of the electron and hole wave functions in the short-period SL's makes features attributed to the type-I–type-II transition hardly observable in the exciton Zeeman splitting. This is clear from Fig. 6(b), where the excellent agreement between the experimental splitting and that calculated in the Kronig-Penney model for the 40-Å-period SL is demonstrated.

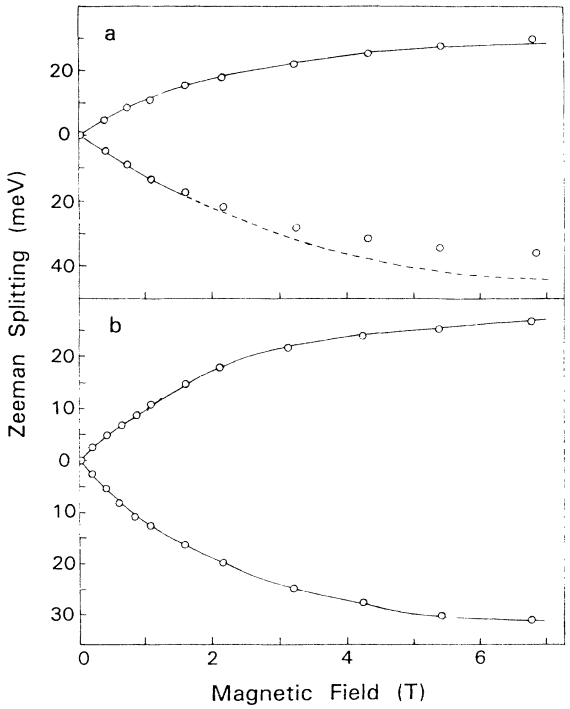

FIG. 6. Zeeman splitting of the heavy-hole exciton in an 18-Å-thick SQW (a) and a 40-Å-period SL (b) with $x=0.1$. Curves are calculated with use of Eq. (30) and parameters $T_{AF}=2.4$ K, $\bar{x}=0.05$, or 0.07 for SQW or SL, respectively.

The longitudinal-transverse splitting of the σ^+ component in an 18-Å-thick SQW as a function of external magnetic fields is shown by closed circles in Fig. 7. A decrease of the LT splitting from 9.0 meV at zero field to 2.3 meV at high magnetic fields can be seen; that is, the oscillator strength is decreased by a factor of 4, signaling the hole confinement in the barrier layers.

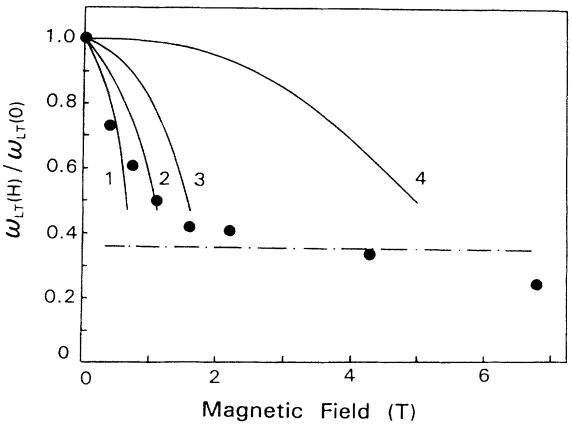

FIG. 7. Normalized oscillator strength of the low-energy (σ^+) Zeeman component of the heavy-hole exciton (closed circles) as a function of an external magnetic field in an 18-Å-thick SQW. Solid curves were computed with use of Eqs. (5) and (6) and the valence-band offsets: 1–15, 2–20, 3–25, and 4–50 meV. Dashed-dotted line—the normalized oscillator strength of an exciton formed by a 3D hole and 2D electron computed using Eq. (35).

According to Eq. (34) at the particular magnetic field of 1.3 T the exciton with $j=1$ can be considered approximately as formed by a 2D electron with the in-plane effective mass m_e^a and a 3D hole with the masses $m_{zz}=m_{\rm hh}$, $m_x=m_{yy}=m_h^{\perp}$. Choosing a trial function in the form

$$\varphi_{\rm SQW}(\rho,z_e,z_h)=\frac{1}{\sqrt{\pi a_{\parallel}a_{\perp}^2}} \times\exp\left[-\left[\frac{z_h^2}{\alpha_{\parallel}^2}+\frac{\rho^2}{a_{\perp}^2}\right]^{1/2}\right]U_e(z_e)$$

and approximating $U_e(z)$ by $(2/a)^{1/2}\cos(\pi z/a)$, we arrive in this case at

$$\omega_{\rm LT}^{\rm SQW}(\sigma^+)=\frac{32}{\pi^2}\frac{e^2|p_{cv}|^2}{\hbar\omega_0^2 m_0^2\epsilon_b}\frac{1}{a_{\parallel}a_{\perp}^2}\ . \tag{35}$$

Here $\omega_{\rm LT}^{\rm SQW}(\sigma^+)$ is the oscillator strength for a SQW exciton with the angular moment component $j=1$ and $a_{\parallel},a_{\perp}$ coincide with the parameters of a similar variational solution for a 3D exciton with the reduced effective masses $\mu_{\perp}$ and $\mu_{\parallel}\equiv m_{\rm hh}$. Coulomb interaction of an electron strongly confined to the CdTe layer with a 3D hole provides $\omega_{\rm LT}^{\rm SQW}$ computed by use of Eq. (35) and shown in Fig. 7 by horizontal dashed-dotted line. The experimental values of the LT splitting tends to arrive the horizontal line at $H\geq H_0$. Moreover, a further decrease of the oscillator strength found at fields higher than 4 T directly indicates the heavy-hole confinement to the $Cd_{1-x}Mn_xTe$ layers. We consider Fig. 7 as a convincing demonstration of the magnetic-field-induced transition from a type-I to a type-II heterostructure for the exciton state $|-\frac{1}{2},\frac{3}{2}\rangle$ contributed to the (σ^+,σ^+) reflection. The figure also includes results of our calculation based on Eqs. (5) and (6) for a number of valence-band offsets. A comparison of these results with a strong quenching of the oscillatory strength observed at $H<H_0$ shows that this effect is very sensitive to the valence-band offset.

A pronounced effect of the transition from a type-I to a type-II SL on the exciton oscillator strength is also found in a 40-Å-period SL. As we conclude based on the data of Fig. 5, an exciton is formed from the 3D-miniband electron and hole in this SL. The observed behavior of the oscillator strength for the high-energy σ^- component, shown by the open circles in Fig. 8, provides evidence that the magnetic-field-induced increase in the barrier heights appears too weak to destroy either the electron or hole miniband. This is in agreement with results of our calculation, shown by the dashed line.

The oscillator strength of the σ^+ component reveals nonmonotonic behavior reducing to the minimal value at $H_0\approx 1.3$ T and increasing at higher fields to values even larger than $\omega_{\rm LT}^{\rm SL}$ at $H=0$ (Fig. 8, closed circles). This effect is governed by changing the offset sign for holes with $m=\frac{3}{2}$ and described by the hole-miniband mass behavior: it is minimal at $H=H_0$ and increases at higher fields as a result of the hole localization in the $Cd_{1-x}Mn_xTe$ layers. Some deviations from the theory shown by the solid curve in Fig. 8 from the experimental

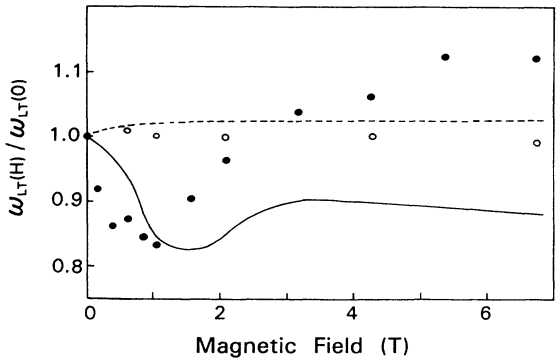

FIG. 8. Normalized oscillator strength of the σ^+ (closed circles) and σ^- (open) Zeeman components as a function of an external magnetic field in a 40-Å-period SL with $x=0.1$. Results of our calculation with $m_e^a=m_e^b=0.1m_0$ and $m_{\rm hh}^a=m_{\rm hh}^b=m_0$ are shown by solid and dashed lines.

data can be attributed to a difference of mass values in the CdTe and $Cd_{1-x}Mn_xTe$ layers, which is neglected in this calculation. The above result shows clearly the spin-dependent redistribution of the hole wave function between the adjacent layers that is the magnetic-field-induced spin SL formation in the $CdTe/Cd_{0.9}Mn_{0.1}Te$ system.

Figure 9(a) displays the oscillator strength behavior of the exciton Zeeman components in a 60-Å-period SL's. In accordance with the results of our calculation shown by the solid curve in Fig. 9(a), the effect of the type-I–type-II transition on the exciton oscillator strength is less remarkable in the 60-Å-period SL (closed circles for

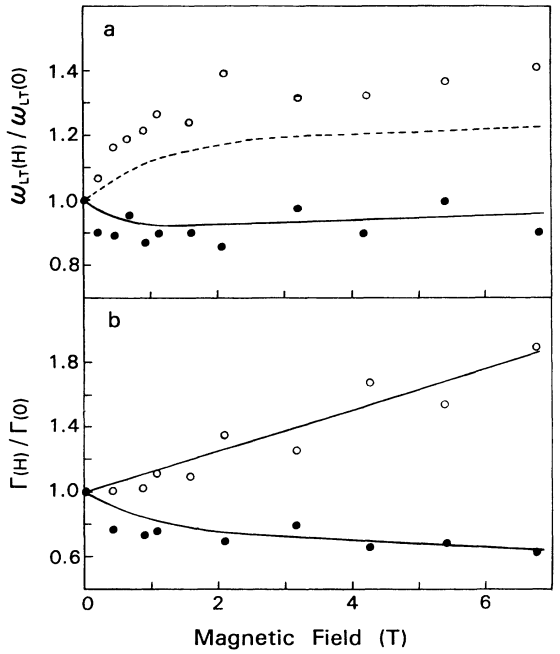

FIG. 9. Normalized oscillator strength (a) and damping (b) of the σ^+ (closed circles) and σ^- (open) components as a function of magnetic field in a 60-Å-period SL with $x=0.1$. The dashed and solid curves in (a) were calculated with $m^a=m^b$ for electrons and for heavy holes. The lines in (b) are guides for the eye.

the σ^+ component). At the same time, a more pronounced effect of the magnetic field is found on $\hbar\omega_{LT}$ of the σ^- component shown by the open circles in Fig. 9(a). An increase in the barrier heights causes a destruction of the electron and hole minibands and the exciton oscillator strength enhancement in qualitative agreement with results of our calculation shown by the dashed line. The theoretical dependence predicts smaller oscillator strengths than those observed. This disagreement seems to be avoided by taking into account an additional hole confinement originating from the 2D electron Coulomb interaction. In Figs. 9(a) and 9(b) we compare the magnetic-field dependences of the exciton oscillator strength and damping [see Eq. (33)]. An increase of the oscillator strength for the σ^- component is accompanied by that of damping, while the oscillator strength and damping of the σ^+ component decrease slowly in the presence of magnetic fields. The observed correlation between these dependences can be understood by taking into account that an increase (decrease) in the barrier heights and, consequently, in the confinement strength causes an enhancement (quenching) of the oscillator strength as well as that of the effect of the layer width fluctuations on the exciton damping. Our findings, based on the resonance reflectivity studies of the exciton longitudinal-transverse splitting and damping, demonstrate clearly the magnetic-field-induced 3D-2D transition in short-period SL's.

V. CONCLUSIONS

In this paper, we have considered several noteworthy examples demonstrating the opportunities to study the magnetic-field-induced changing of band characteristics like miniband widths and band offsets by resonance reflection spectroscopy. Monitoring the exciton oscillator strength in SQW's as a function of the well width has allowed us to reveal an additional hole confinement in the adiabatic Coulomb potential which dominates in QW's thicker than 30 Å.

To avoid the above effect on the oscillator strength behavior, we have demonstrated the magnetic-field-induced transition from a type-I to a type-II heterostructure for heavy holes in an 18-Å-thick SQW and the spin superlattice formation in a 40-Å-period SL with the 3D character of the electron wave function.

In addition, we have studied the transition from the 3D to 2D character of the exciton wave function in the short-period SL's, monitoring the exciton oscillator strength and damping as a function of the barrier heights tuned by varying an externally applied magnetic field.

ACKNOWLEDGMENT

This work has been supported in part by the Bundesministerium für Forschung und Technologie, Bonn.

*On leave from A. F. Ioffe Physico-Technical Institute, Russian Academy of Sciences, 194021 St. Petersburg, Russia.

[1]S. K. Chang, A. V. Nurmikko, J. W. Wu, L. A. Kolodziejski, and R. L. Gunshor, Phys. Rev. B **37**, 1191 (1988).

[2]E. Deleporte, J. M. Berroir, G. Bastard, C. Delalande, J. M. Hong, and L. L. Chang, Superlatt. Microstruct. **8**, 171 (1990); Phys. Rev. B **42**, 5891 (1990).

[3]B. Kuhn, W. Ossau, A. Waag, R. N. Bicknell-Tassius, and G. Landwehr, J. Cryst. Growth **117**, 871 (1992).

[4]Al. L. Efros, Fiz. Tekh. Poluprovodn. **20**, 1281 (1986) [Sov. Phys. Semicond. **20**, 808 (1986)].

[5]G. R. Pozina, A. V. Kavokin, V. P. Kochereshko, I. N. Uraltsev, D. R. Yakovlev, G. Landwehr, R. N. Bicknell-Tassius, and A. Waag, Solid State Commun. **81**, 639 (1992); J. Cryst. Growth **117**, 877 (1992).

[6]J. W. Wu, and A. V. Nurmikko, Phys. Rev. B **38**, 1504 (1988).

[7]G. Peter, E. Deleporte, G. Bastard, J. M. Berroir, C. Delalande, B. Gil, J. M. Hong, and L. L. Chang, J. Lumin. **52**, 147 (1992).

[8]D. R. Yakovlev, W. Ossau, G. Landwehr, R. N. Bicknell-Tassius, A. Wang, and I. N. Uraltsev, Solid State Commun. **76**, 325 (1990); Surf. Sci. **263**, 485 (1992).

[9]A. V. Kavokin and K. V. Kavokin, Semicond. Sci. Technol. (to be published).

[10]M. Kohl, M. R. Freeman, J. M. Hong, and D. D. Awschalom, Phys. Rev. B **43**, 2431 (1991).

[11]A. Wasiela, Y. Merle d'Aubigne, J. E. Nicholls, D. E. Ashenford, and B. Lunn, Solid State Commun. **76**, 263 (1990).

[12]N. Dai, H. Luo, F. C. Zhang, N. Samarth, M. Dobrowolska, and J. K. Furdyna, Phys. Rev. Lett. **67**, 3824 (1991).

[13]W. C. Chou, A Petrou, J. Warnock, and B. T. Jonker, Phys. Rev. Lett. **67**, 3820 (1991).

[14]E. L. Ivchenko, P. S. Kopev, V. P. Kochereshko, I. N. Uraltsev, D. R. Yakovlev, S. V. Ivanov, B. Ya. Meltser, and M. A. Kalitievskii, Fiz. Tekh. Poluprovodn. **22**, 497 (1988) [Sov. Phys. Semicond. **22**, 302 (1988)].

[15]E. L. Ivchenko, V. P. Kochereshko, and I. N. Uraltsev, in *Studies in A. F. Ioffe Physico–Technical Institute* (Nova Science, New York, 1992), Vol. 15.

[16]L. C. Andreani, F. Tassone, and F. Bassani, Solid State Commun. **77**, 641 (1991).

[17]E. L. Ivchenko, Fiz. Tverd. Tela (Leningrad) **33**, 2388 (1991) [Sov. Phys. Solid State **33**, 1344 (1991)].

[18]E. L. Ivchenko and A. V. Kavokin, Fiz. Tverd. Tela (Leningrad) (to be published) [Sov. Phys. Solid State (to be published)].

[19]V. M. Agranovich and O. A. Dubovski, Pis'ma Zh. Eksp. Teor. Fiz. **3**, 345 (1966) [JETP Lett. **3**, 223 (1966)].

[20]E. L. Ivchenko, V. P. Kochereshko, P. S. Kopev, V. A. Kosobukin, I. N. Uraltsev, and D. R. Yakovlev, Solid State Commun. **70**, 529 (1989).

[21]L. C. Andreani and F. Bassani, Phys. Rev. B **41**, 7536 (1990).

[22]E. L. Ivchenko, in *Excitons*, edited by E. I. Rashba and M. D. Sturge (North-Holland, Amsterdam, 1982), p. 141.

[23]E. L. Ivchenko and A. V. Kavokin, Fiz. Tekh. Poluprovodn. **25**, 1780 (1991) [Sov. Phys. Semicond. **25**, 1070 (1991)].

[24]J. A. Gaj, R. Planel, and G. Fishman, Solid State Commun. **29**, 435 (1979).

[25]A. Waag, S. Schmeusser, R. N. Bicknell-Tassius, D. R. Yakovlev, W. Ossau, G. Landwehr, and I. N. Uraltsev, Appl. Phys. Lett. **59**, 2995 (1991).

[26]Y. Merle d'Aubigné, L. S. Dang, A. Wasiela, N. Magnea, F. Dal'bo, and A. Million, J. Phys. (Paris) Colloq. **48**, C5-363 (1987).

[27]B. Kuhn-Heinrich, W. Ossau, M. Popp, E. Bangert, A. Waag, and G. Landwehr (unpublished).